Neutron Beam Effects on Spin-Exchange-Polarized ^{3}He

M. Sharma*,[1] E. Babcock,[2] K.H. Andersen,[2] L. Barrón-Palos,[3,4] M. Becker,[2,5] S. Boag,[6] W.C. Chen,[7] T.E. Chupp,[1] A. Danagoulian,[8] T.R. Gentile,[7] A. Klein,[8] S. Penttila,[9] A. Petoukhov,[2] T. Soldner,[2] E.R. Tardiff,[1] T.G. Walker,[10] and W.S. Wilburn[8]

[1] *FOCUS Center and Physics Department, University of Michigan, Ann Arbor, MI 48104, USA*
[2] *Institut Laue Langevin, BP 156, 38042 Grenoble Cedex 9, France*
[3] *Arizona State University, Tempe, AZ 85287 USA*
[4] *Universidad Nacional Autónoma de México, México, D.F. 04510, México*
[5] *Physikalisches Institut, Universität Heidelberg, Philosophenweg 12, 69120 Heidelberg, Germany*
[6] *ISIS, Rutheford Appelton Labs, Chilton, Didcot OX11 0QX, UK*
[7] *National Institute of Standard and Technology,Gaithersburg, MD 20899-8461, USA*
[8] *Los Alamos National Lab, Los Alamos, NM 87545 USA*
[9] *Oak Ridge National Lab, Oak Ridge, TN 37831 USA*
[10] *University of Wisconsin, Madison, WI 53706 USA*

(Dated: February 21, 2008. To be submitted to Phys. Rev. Lett.)

We have observed depolarization effects when high intensity cold neutron beams are incident on alkali-metal-spin-exchange polarized ^{3}He cells used as neutron spin filters. This was first observed as a reduction of the maximum attainable ^{3}He polarization and was attributed to a decrease of alkali-metal polarization, which led us to directly measure alkali-metal polarization and spin relaxation over a range of neutron fluxes at LANSCE and ILL. The data reveal a new alkali-metal spin-relaxation mechanism that approximately scales as $\sqrt{\phi}_n$, where ϕ_n is the neutron capture-flux density incident on the cell. This is consistent with an effect proportional to the recombination-limited ion concentration, but is much larger than expected from earlier work.

PACS numbers: 32.80.Xx, 24.70.+s, 03.75.Be, 61.80.Hg

Polarized gaseous ^{3}He has wide application including targets and beams for nuclear physics measurements, for electron scattering studies of the structure of the neutron[1], for biomedical imaging of the airspace in the lungs[2], and as a neutron polarizer[3, 4, 5]. Each of these applications has a different set of requirements and acceptable tradeoffs of polarization, density, size and polarization stability. There are two techniques used to produce polarized ^{3}He gas: metastability exchange optical pumping (MEOP) and spin-exchange optical pumping (SEOP). MEOP polarizes pure ^{3}He at low pressure, typically 1 mbar, at rates of about 1 bar-liter/hour with ^{3}He polarizations of 70% or more[5]. MEOP polarizer stations compress the ^{3}He into cells that are transported to the point of use where the ^{3}He polarization decays very slowly, with a time constant that can be a week or longer[6]. For SEOP, the ^{3}He is polarized by the hyperfine interaction during collisions of the ^{3}He nuclei with polarized valence electrons of optically pumped alkali-metals. Production rates with SEOP are about an order of magnitude lower than the highest MEOP rates but similarly high ^{3}He polarizations have been acheived[7]. For applications that require several days or weeks of stable high polarization operation, such as targets for electron scattering, neutron scattering instruments with limited access, and long-running fundamental neutron physics experiments, it is practical to have a SEOP system pumping continuously, with stable polarization, for weeks or months [4, 8].

Gaseous polarized ^{3}He is used for polarized neutron measurements because of the nearly complete spin-dependence of the absorption cross section for the process ^{3}He(n,p)^{3}H+764 keV. This proceeds through an unbound 0^+ resonance in ^{4}He, so that only neutrons with spin opposite to the ^{3}He spin are absorbed[9]. The effective absorption cross section for neutrons of wavelength λ can be written

$$\sigma_a = \sigma_0 \frac{\lambda}{\lambda_0} \frac{1 \mp P_3}{2}, \tag{1}$$

for neutron spin parallel ($-$) or antiparallel ($+$) to the ^{3}He polarization. Here $\sigma_0 = 5333 \pm 7$ b is the absorption cross section for thermal neutrons ($\lambda_0 = 1.8$ Å)[10], and P_3 is the magnitude of the ^{3}He polarization. In a spin-filter polarizer, the ^{3}He polarization is not complete, and neutrons of both spin states are absorbed, though with different absorption lengths. Thus the wavelength dependent transmission and polarization of the neutrons are given by

$$T_n(\lambda) = e^{-\sigma_0 t_3 \frac{\lambda}{\lambda_0}} \cosh(P_3 \sigma_0 t_3 \frac{\lambda}{\lambda_0}),$$

$$P_n(\lambda) = \tanh(P_3 \sigma_0 t_3 \frac{\lambda}{\lambda_0}), \tag{2}$$

where t_3 is the ^{3}He areal density. Transmission of polarized neutrons through polarized ^{3}He can also be used to analyze the neutron polarization with an analyzing power $A_n = \tanh(P_3 \sigma_0 t_3 \frac{\lambda}{\lambda_0})$.

In a typical SEOP neutron spin filter, the ^{3}He cells are constructed from boron-free glass, *e.g.* GE180[11]. Alkali-metal (rubidium[12] or a mixture of rubidium and potassium[13]) is distilled into the cell with about one bar of ^{3}He at room temperature and a small amount of N_2 added to suppress radiation trapping, the multiple scattering of optical pumping photons that depolarize the alkali-metal atoms[14]. The cell is heated to maintain an optimum alkali-metal vapor pressure, held in a magnetic field of 10-30 Gauss, and illuminated by a high powered laser tuned to the rubidium D1 resonance at 794.7 nm. The ^{3}He polarization is governed by an exponential time dependence with rate constant and equilibrium polarization given respectively by

$$\Gamma = (1 + X_{cell})\gamma_{SE} + \Gamma_R \qquad P_3^{eq} = P_A \frac{\gamma_{SE}}{\Gamma} \qquad (3)$$

where $\gamma_{SE} = \langle \sigma_{SE} v \rangle$[Rb], the velocity-averaged spin-exchange rate constant, is typically $1/(10 - 15$ h). The ^{3}He relaxation rate, Γ_R, is a sum of rates due to cell wall interactions, impurities, ^{3}He dipole-dipole relaxation, magnetic field gradients and ionization effects. The rate Γ_R is generally 10-50 times smaller than γ_{SE}. The volume averaged alkali metal electron polarization is P_A, and the factor X_{cell} accounts for an observed reduction in ^{3}He polarization that varies from cell-to-cell [18].

Neutron beam effects on the ^{3}He polarization were first observed during development of the NPDGamma experiment at the Los Alamos Neutron Science Center (LANSCE)[4, 15] and were further studied in dedicated runs at LANSCE and at the Institute Laue-Langevin (ILL) in Grenoble. The ^{3}He polarization for a cell used at LANSCE over two months is shown in Figure 1. The cells and set-up are described in reference [4]. The top panel shows that, though the ^{3}He polarization appears relatively constant over the long term (except for the period with the laser off), there is a slow downward drift. The long time constant decay of ^{3}He polarization appears to be due to a milky white coating that builds up on the cell walls and reduces transmission of laser light into the cell[4]. This build-up is probably due to rubidium compounds, possibly due to reaction with the hydrogen (^{1}H and ^{3}H) produced by neutron absorption on ^{3}He. A similar effect was observed for a pure rubidium cell at 170°C placed in the full flux PF1B beam at ILL for one hour. Exposure for one hour at PF1B is equivalent to about three days at LANSCE FP12. A Monte Carlo calculation based on the measured brightness of the LANSCE neutron source [16] predicts a maximum capture-flux density of $1 - 3 \times 10^8$ cm^{-2}s^{-1}. (Capture flux, the integral of the $1/v$ weighted neutron intensity spectrum, is proportional to the total neutron capture or decay rate per unit length.) The PF1B capture-flux density at the cell position was measured with gold foils and found to be 1.4×10^{10} cm^{-2}s^{-1}. The PF1B beam is

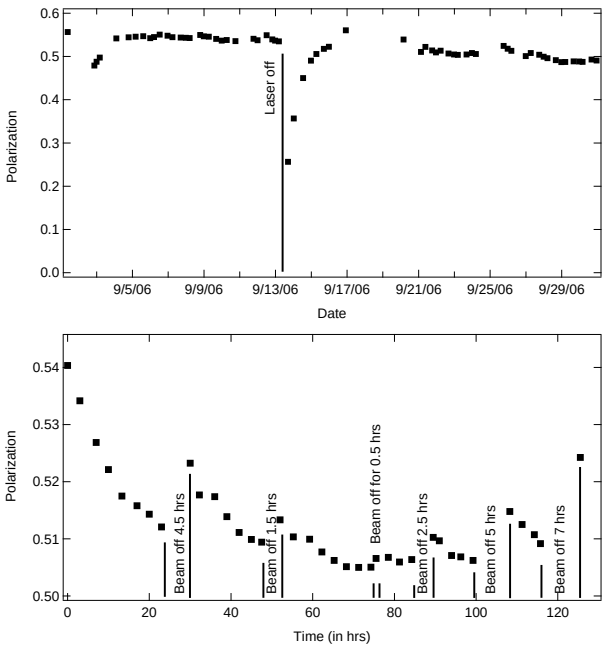

FIG. 1: LANSCE neutron spin filter ^{3}He polarization. The top panel shows the long term behavior; the bottom panel shows the effect of the neutron beam on short time scales.

described in reference [17]

Data for P_3 on shorter time scales are shown in the bottom panel of Figure 1. When the beam is on, the ^{3}He polarization decays, and with the beam off, the polarization recovers, at least partially. The short time-scale data of Figure 1 show that the neutron beam causes the ^{3}He polarization to decay to a lower value of P_3^{eq} at a rate of approximately (1/12 h), which is consistent with the measured Γ. The polarization was not measured with the neutron beam off, because we used the neutrons to measure P_3 [4]; however the increase of ^{3}He polarization is consistent with a similar rate constant. Since Γ does not change appreciably, the most likely cause is a drop of P_A, possibly due to ionization effects induced by the neutron beam. Ionization effects on both Γ and P_A were observed in work with a 180 particle-nA beam of 18 MeV alpha particles[19]. Those observations led to the development of the double cell now ubiquitous in SEOP based polarized ^{3}He targets for electron scattering [20]; however we expected these effects to be negligible for ^{3}He cells in neutron beams, where the ionization energy loss is 100 to 10,000 times less. We therefore set out to measure the effects of the neutron beam on the alkali-metal polarization in high-flux neutron beams under a range of conditions.

The volume averaged alkali-metal polarization was directly measured using electron-spin resonance (ESR)[21] at both LANSCE and ILL. In the LANSCE set-up the transmission of optical pumping light from a single 30 W broadband laser-diode array was monitored as RF at

14 MHz was applied and the magnetic field swept from 28.4 to 29.0 Gauss. The magnetic field was produced by the combination of a very uniform 10 Gauss field from a large set of coils and a pair of hand-wound rectangular coils that produced a less homogeneous field of about 20 Gauss. The consequence of the inhomogeneity is that the ESR lines are broadened so that the hyperfine lines are not all separately resolved. Data for two different neutron beam intensities and no beam are shown in Figure 2. When the hyperfine levels are not resolved, the rubidium polarization is given by $P_A = (7R-3)/(7R+3)$ for ^{85}Rb ($I = 5/2$), where R is the ratio of adjacent ESR peak areas extrapolated to zero RF power.

For the ILL set up, the ESR measurements were made at 10 Gauss with a hybrid Rb-K cell constructed at NIST [7]. The second-order Zeeman splitting of the potassium is much larger than that of rubidium and allows ESR of ^{39}K to be resolved at 10 Gauss as shown in Figure 3. The signals from ^{87}Rb, and ^{41}K[13] (both $I = 3/2$) are also observed. Rapid spin exchange between the rubidium and potassium[22] allows the ESR of potassium to measure the average electron polarization of all the alkali-metal species. The cell was illuminated with light from two 100 Watt narrowed diode-laser-array bars[23]. A linearly polarized probe laser, tuned near the Rb D2 resonance and directed along the magnetic field, was used to measure the Faraday rotation signal, which is proportional to the alkali-metal polarization along the probe beam path through the vapor[24]. The RF field was swept over a range of approximately 1.1 MHz around 7.6 MHz and the data extrapolated to zero RF power. For $I = 3/2$ $P_A = (2R-1)/(2R+1)$.

The alkali-metal polarization at any position in the cell, is given by[12]

$$\frac{1}{P_A(\vec{r})} = 1 + \frac{\Gamma_{SD}}{\gamma_{opt}(\vec{r})}, \tag{4}$$

where $\gamma_{opt}(r)$ is the convolution of the laser spectral profile and the optical absorption cross section at the position $\vec{r}$. The spin destruction rate, Γ_{SD}, is the rate of electron spin-flips per alkali-metal atom and most likely changes more significantly than $\gamma_{opt}(\vec{r})$. In Figure 4 we plot the change $\Delta(1/P_A)$ relative to no beam as a function of neutron capture-flux density, ϕ_n, for both the LANSCE and ILL data. With the higher power, narrowed lasers pumping the hybrid cell at ILL, the neutron-beam effects are significantly reduced compared to the LANSCE data at a given neutron flux density.

Relaxation of the alkali-metal polarization was studied at ILL using the relaxation in the dark technique [26]. A small alkali-metal polarization was produced by a low power optical pumping beam (less than 0.1W/cm^2), which was chopped at 1 Hz. The polarization, P_A, was measured by Faraday rotation with the same setup used for the data shown in Figure 3. With the optical-pumping beam chopped off, the polarization decayed at

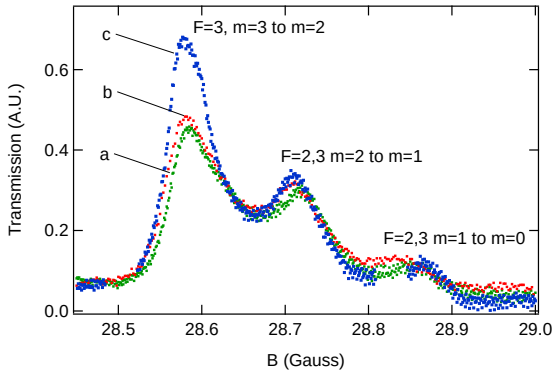

FIG. 2: ESR spectra of ^{85}Rb for full flux (a: green) and 19% of full flux (b: red) and no beam (c: blue) at LANSCE. The polarizations are $P_A = 0.6$, 0.64 and 0.7, respectively. The relative uncertainties, estimated to be 1-2%, are limited by the signal-to-noise ratio of the ESR measurements.

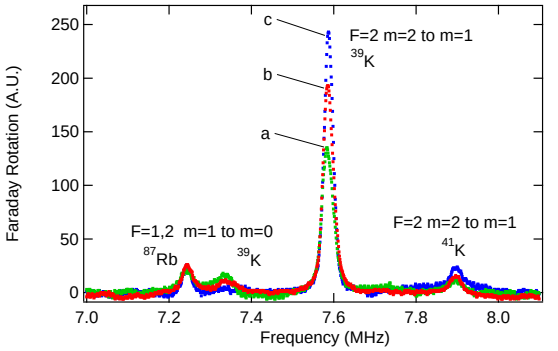

FIG. 3: ESR Spectra of ^{39,41}K and ^{87}Rb ESR for full flux (a: green) and 8.5% of full flux (b: red) and no flux (c: blue) at ILL. The polarizations are $P_A = 0.83$, 0.90, 0.98, respectively.

a rate $\Gamma_A = \Gamma_{SD}/S$, where the slowing factor $S \geq 1$ accounts for the angular momentum stored in the nuclear spins, which couple to the electron spin through the hyperfine interaction[27]. Due to electron spin-exchange, the factor S is an average over isotopes and alkali-metal species. The slowing factor depends on the alkali-metal polarization; for low polarization, $S = 10.8$ for natural rubidium[27], and $S = 6$ for potassium[13]. Results for $\Delta\Gamma_A$, the neutron-flux contribution to the relaxation rate, for all five cells measured at ILL, each with different gas and alkali-metal compositions, are shown in Figure 5. With no beam, Γ_A varies from 20 to 30 s^{-1} depending on gas and alkali-metal compositions and pressures. The solid line in Figure 5 has the form $\Delta\Gamma_A \propto \sqrt{\phi_n}$. As shown below, this would be consistent with relaxation due to a recombination-limited equilibrium ion concentration.

The processes due to the ionization, created mainly by the ^{3}He(n,p)^{3}H reaction, are complex and involve ions, metastable ^{3}He atoms, molecular ions and radicals of helium and nitrogen. One or more of these species may be

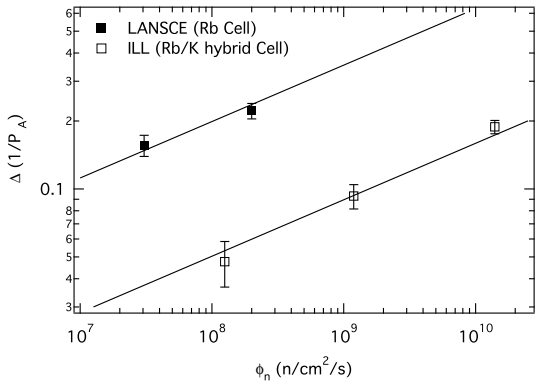

FIG. 4: Neutron induced change in polarization for the LANSCE Rb cell and ILL hybrid cell. The solid lines are provided to guide the eye.

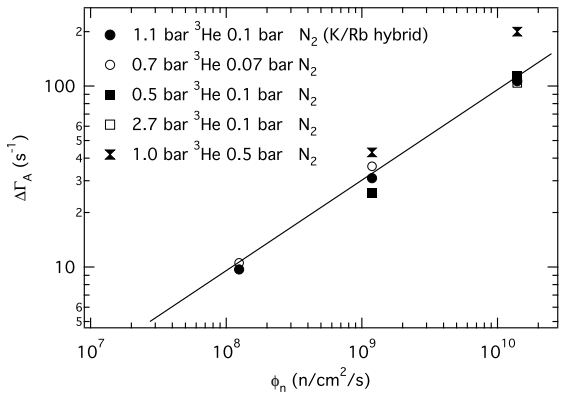

FIG. 5: ILL polarization relaxation results for r all cells. Error bars of ≈10% are similar to the size of the symbols. The solid line, provided to guide the eye, is proportional to $\sqrt{\phi_n}$.

the cause of the observed effects. We consider the simplified case of production of an ion species of density n_i at a rate proportional to the neutron capture-flux density ϕ_n: $\frac{dn_i}{dt} = \gamma\phi_n - \beta n_i$, where γ=(764 keV/δE_i)/L for a cell of length L, δE_i is the energy cost per ion-pair (*e.g.* δE_i=32.5 eV for helium), and β is the rate constant for recombination due all mechanisms including electron recombination, neutralization at the cell wall, and charge exchange with species that do not contribute to ΔP_A ($\beta = \beta_e + \beta_W + \beta_{ex} + \ldots$). In the limit that electron recombination is dominant, the equilibrium electron density will be proportional to n_i, *i.e.* $\beta_e = \alpha n_i$, and the equilibrium solution is, $n_i = \sqrt{\gamma\phi_n/\alpha}$, consistent with the solid line in Figure 5.

In summary, measurements at LANSCE and ILL with in-situ SEOP ^{3}He neutron spin filters have shown that the incident neutron beam induces an decrease of alkali-metal polarization and a corresponding increase of the alkali-metal relaxation rate. Measurements over several decades of neutron flux show that the increased spin relaxation rate approximately scales with $\sqrt{\phi_n}$, which would be consistent with the recombination-limited equilibrium concentration of one or more ion species. The magnitude of this effect is much larger than expected given earlier study of ionization effects produced by an alpha-particle beam[19]. At ILL's PF1B, the world's highest flux cold neutron beam for fundamental physics, P_A was reduced by about 20% in a potassium-rubidium hybrid cell pumped by high-power narrowed diode laser arrays. Further neutron-beam related effects were observed in the ILL measurements including a combination of prompt and delayed changes in the alkali-metal relaxation rates, cell pressure dependent effects and performance of a double cell. These will be presented in a separate paper.

This work was supported by the U. S. National Science Foundation, the Department of Energy, the ILL Millennium Programme, and the NMI3. We gratefully acknowledge the efforts of the entire NPDGamma collaboration in developing the apparatus used to provide the data shown in Figure 1, and we gratefully acknowledge the technical assistance of the ILL ^{3}He group.

[1] T. Chupp *et al.*, Ann. Rev. Nuc. Part. Sci. **72**, 373 (1994).
[2] H.U. Kauczor *et al.*, European Radiology **8**, 820 (1998).
[3] K.P. Coulter *et al.*, Nucl. Inst. Meth. A **288**, 463 (1990).
[4] T.E. Chupp *et al.*, Nucl. Inst. Meth. A **574**, 500 (2007).
[5] A. Petoukhov *et al.*, Physica B **385-386**, 1146 (2006).
[6] K.H. Andersen *et al.*, Physica B **385-386**, 1134 (2006).
[7] W.C. Chen, T.R. Gentile, T.G. Walker, and E. Babcock, Phys. Rev. **A 75**, 013416, (2007).
[8] J.R. Johnson *et al.*, Nucl. Inst. Meth. A **356**, 148 (1995).
[9] L. Passell, R.I. Schermer, Phys. Rev. **150**, 146 (1966).
[10] S.F. Mughabghab *et al.*, **Neutron Cross Sections**, Academic Press, New York (1981).
[11] G. L. Jones *et al.*, Nucl. Inst. Meth. A **440**, 772 (2000).
[12] T.E. Chupp *et al.*, Phys. Rev. **C 36**, 2244 (1987).
[13] E. Babcock *et al.*, Phys. Rev. Lett. **91**, 123003, (2003).
[14] T.E. Chupp, K.P. Coulter, Phys. Rev. Lett. **55**, 1074 (1985).
[15] M. Gericke *et. al.*, Phys Rev. **C74**, 065503 (2006).
[16] P. Seo *et al.*, Nucl. Inst. Meth. A **517**, 285 (2004).
[17] H. Abele *et al.*, Nucl. Inst. Meth. A **562**, 407 (2006).
[18] E. Babcock *et al.*, Phys. Rev. Lett. **96**, 083003, (2006).
[19] K.P. Coulter *et al.*, Nucl. Inst. Meth. A **276**, 29 (1989).
[20] T.E. Chupp *et al.*, Phys. Rev. **C45**, 915-930 (1992).
[21] E. Babcock *et al.*, Phys. Rev. **A 71**, 013414, (2005).
[22] L.W. Anderson *et al.*, Phys. Rev. Lett. **120**, 1279 (1960).
[23] B. Chann *et al.*, J. Appl. Phys. **94**, 6908 (2003).
[24] E. Vliegen *et al.*, Nucl. Inst. Meth. A **460**, 444-50 (2001).
[25] M.E. Wagshul, T.E. Chupp, Phys. Rev., **A40**, 4447 (1989).
[26] W. Franzen, Phys. Rev., **115**, 850 (1959).
[27] M.E. Wagshul, T.E. Chupp, Phys. Rev. A **49**, 3854 (1994).
[28] K.D. Bonin *et al.*, Phys. Rev. **A**, 3270 (1988).
[29] R.G. Milner *et al.*, Nucl. Inst. Meth. S **257**, 286 (1987).